Walking on chains: The morphology and mechanics behind the fin ray derived limbs of sea-robins

Jarrod C. Petersen*[1,2] and Jason B. Ramsay[1]

1. Biological Department, College of Mathematics and Sciences, Westfield State University, 577 Western Avenue, Westfield, MA 01086
2. Present Address: Department of Ecology and Evolutionary Biology, Brown University, 80 Waterman Street, Providence, RI 02912

*Author for correspondence (jarrod_petersen@brown.edu)

Keywords: Fin rays, *Prionotus*, Locomotion, Lepidotrichia, Materials, Fish

Summary: Our results highlight several morphological modifications that likely contribute to the stiffness of the novel walking appendages in the sea-robin and therefore their ability to facilitate underwater locomotion.

ABSTRACT

Fish fin rays (lepidotrichia) are typically composed of paired and segmented flexible structures (hemitrichia) that help support and change the shape of the fins to affect water flow. Yet, marine ray-finned fish that are members of the family Priontinae (sea-robins) have specialized pectoral fin rays that are separated from the fin and used as limbs to walk along the seafloor. While previous kinematic studies have demonstrated the use of these specialized fin rays as walking appendages, there is little information on how the morphology of the "walking-rays" and associated musculature facilitate underwater walking. Here, we examine the musculoskeletal anatomy of the walking and pectoral fin rays in striped sea-robin, *Prionotus evolans* and compare the mechanical properties of the rays with those of the smaller northern sea-robin, *Prionotus carolinus*. We aimed to determine what structural modifications in the walking-rays allow them to function as a supportive limb. We found enlarged processes for muscle attachment, bone extensions that brace the hemitrich articulations, and reduced flexibility and increased second moment of area along the rostro-caudal bending axis in the rays used for walking. This novel limb design may have promoted the benthic foraging behavior exhibited by these species by uncoupling locomotion and feeding.

INTRODUCTION

Underwater walking has evolved independently many times over the course of evolutionary history and is the main mode of locomotion in many arthropods (Hu and Bush, 2010), echinoderms (Hennebert et al., 2010), skates and rays (Bilecenoglu and Ekstrom, 2013), and bony fish (Edwards, 1989). Though these phylogenetically distinct groups use different mechanisms to walk, walking fish exhibit one commonality: their whole fin or the majority of the fin is used as a walking appendage (Bilecenoglu and Ekstrom, 2013; King et al., 2011). Within the bony fish class, Triglidae (sea-robins) are fish that forage on the benthos. They have evolved a unique mechanism for walking underwater and they exhibit features used for walking that differ from those common to the Osteichthyes mentioned. The first three fin rays (lepidotrichia) of the leading edge of the pectoral fin on each side of the body have separated and comprise the six leg-like structures, used as individual limbs, that allow sea-robins to walk along the seafloor (Eudes-Deslongchamps, 1843; Morrill, 1895; Renous et al., 2000)(Fig. 1). Lepidotrichia are typically composed of two parallel segmented bony chains which control the contours of the fins (hemitrichia) that extend proximal to distal along the fin and support the fin membrane (Flammang et al., 2013; Lauder et al., 2006; Walker, 2004). The pectoral lepidotrichia used for walking in sea-robins, which will be referred to as the walking-rays (WR) throughout the rest of the manuscript, have become completely detached from the rest of the fin. This separation allows them to flex and move independently like small fingers or limbs as these fish use them to walk on the seafloor (Renous et al., 2000). Though sea-robins have successfully adopted lepidotrichia for walking, there is an inherent issue with their use in that function. The segmented bone structure of typical hemitrichia allows for flexibility on multiple planes (Walker, 2004; Yano and Tamura, 2013), but without the support of the fin membrane, lepidotrichia may buckle against ground reaction forces and cannot accelerate the body of the fish. In other words, the typical morphology of individual lepidotrichia might impede the transmission of propulsive forces as they flex against the substrate.

While anatomical features of the walking-rays have been described by Eudes-Deslongchamps (1843), Morrill (1895) the majority of the description focuses on the neural anatomy associated with sensory function. A study focusing on the morphology and

comparative ecology of the northern sea-robin, *Prionotus carolinus*, was used as a reference for our morphological analysis (Harris, 2013). Here, we investigate the anatomical and mechanical features of the walking-rays of the striped sea-robin, *Prionotus evolans,* from the perspective of locomotor function. Recent studies have identified the fin rays of fish and fingers of vertebrates, including humans, share a common developmental expression origin (Nakamura et al., 2016; Yano and Tamura, 2013). While this does not indicate homology, our initial observations revealed the walking-rays flex in one direction while resisting flexion in all other directions, much like a digit. Based on that information and the novelty of this structure, we propose the following hypotheses: 1) walking-rays will exhibit more robust skeletal components for support and muscle attachment, and an increased range of motion at the base compared to pectoral fin rays; 2) walking-ray musculature will be separated from the pectoral fin ray musculature and will share morphological similarities with tetrapod distal forelimb musculature. Specifically, they will contain divisions with tendons that travel the length of the ray to insert on the distal most end, as well as ligamentous loops that guide flexion of the walking-rays, similar to the morphology of annular pulleys that influence the action the flexor digitorum superficialis in tetrapods (Doyle, 1988); and 3) ray stiffness will be similar in the walking-rays and pectoral fin rays, suggesting that the walking-rays may be actively reinforced by muscles during walking locomotion.

MATERIALS AND METHODS

Specimens and Morphology

Sixteen sea-robins were used during this study. Those included two preserved, and six freshly frozen specimens of *Prionotus evolans* (Lineaus, 1766) at 33.1 - 37.7cm total length and eight fresh frozen specimens of *Prionotus carolinus* (Lineaus, 1771) at 24.3 – 25.8cm total length. All fresh specimens were obtained from local fishers in Narragansett, Rhode Island USA and used for morphological and mechanical analysis of the walking-rays and associated musculature. All animal use was approved by the Westfield State University Institutional Animal Care and Use Committee.

Observations from gross dissection and CT scans were used to investigate the structure of the walking-ray articulation with the pectoral girdle to detect range of motion differences.

The skeletal morphology of the walking-rays was compared with that of the pectoral fin rays in order to identify functional novelties potentially facilitating the walking function. Both species studied have three walking-rays on each side (Fig. 1), which are designated here as the first, second and third walking-rays ordered rostral to caudal. The skeletal morphology of the walking-rays and associated hemitrichs was examined by gross dissection and micro computed tomography (CT) scanning using the Bruker Microphotonics Skyscan 1173 at the Karel F. Liem Bioimaging center at The University of Washington Friday Harbor Marine Laboratories. The rays from fresh and preserved specimen that were used for CT imaging were tightly wrapped in wet cheesecloth in order to keep them hydrated and immobilized during scanning. The first walking-ray was manipulated into a ventrally flexed position that mimicked the natural position of the ray during locomotion (Renous et al., 2000). After positioning, the ray was tied with a cotton thread attached at the proximal and distal ends of the ray so it would remain flexed during scanning. The second and third walking-rays and a pectoral fin ray were kept straight as if tucked away on the lateral-ventral side of the sea-robin during scanning. Scanning both flexed and straight walking-rays was done in an attempt to reveal any potential changes to the orientation of skeletal elements or interactions at the joints that may occur when the ray is bent during normal locomotion or straightened when swimming. For all anatomical descriptions the rays are described as if they are in a protracted and externally rotated position, which is how they would be positioned during walking.

The morphology of the muscles associated with the walking-rays was examined via gross dissection from fresh and preserved specimen and compared with that of the pectoral fin rays. Superficial and deep muscular divisions associated with the walking-rays were compared with those associated with the pectoral fin rays. All anatomical features were documented photographically using a 12-megapixel Apple digital camera mounted on a Nikon SMZ800 stereo dissecting scope at a magnification range of 10x to 62x.

Manual Manipulations

The walking-rays and pectoral fin rays of fresh specimen were manually manipulated to assess mobility of the individual rays relative the pectoral girdle and the general flexibility of the lepidotrichia on planes relevant to walking behavior within the two species, the ventro-

dorsal and rostro-caudal planes. These planes were chosen due to their biological significance to walking kinematics of sea-robins (Renous et al., 2000). Ligamentous connections were also viewed using the same techniques. Potential muscle function was assessed by pulling muscles down their line of action and observing the resulting motion at the walking-rays. Connective tissue between the hemitrichia during flexion and relaxation was viewed under a Nikon SMZ800 stereo dissecting scope at a magnification range of 40x to 62x. Images were captured through the Nikon DXM1200C mounted camera with ACT-1C software.

Materials Testing

Three-point bending tests were conducted to determine the stiffness of walking-rays and pectoral fin rays. For all tests, rays were supported at two ends on a custom-built rig while a force was applied at the midpoint by a materials testing device (MTS etc.) (Fig. 2A). The first pectoral fin ray and third walking-ray were tested from 10 fresh specimens, four from *P. evolans* and six from *P. carolinus*. Testing was done in two orientations, along the rostro-caudal and ventro-dorsal axes (Fig. 2). These axes correspond to the short axis of the ray in the orientation where the walking-ray is perpendicular to the body and flexed, as in normal locomotion. In the rostro-caudal direction, the mid-point force was applied to the rostral surface of the rays and the support points were in contact with the caudal surface. This was done to mimic the forces present during the caudal sweeping motion of the walking-ray during normal locomotion (Renous et al., 2000). In the ventro-dorsal direction, the force was applied to the ventral surface of the rays and the support points were in contact with the dorsal surface. This was done to mimic the forces present during the flexion of the walking-ray during normal locomotion (Renous et al., 2000). Testworks 4 software was used for data recording and analysis. A constant speed of 1.27mm/minute was used for the three-point bending test, as it matches the normal gait speed of the sea-robin (Renous et al., 2000). The rays were kept hydrated throughout testing, so as not to alter the natural flexibility due to tissue shrinkage from dehydration.

Mechanical Properties

Cross-sectional area was measured at the point of MTS force application to allow for calculation of fin ray material properties. Following testing, the surface of each ray was blotted dry and a mark was added at the point of force application with a 0.5mm tip pen using permanent ink. A 1mm section was cut from the pectoral fin rays and the walking-rays at the marked point using a blade from an American Optical microtome model 820. Cross-sectional images were obtained from the segments using a 12-megapixel Apple digital camera mounted on a Nikon SMZ800 stereo dissecting scope at a magnification range of 40x to 62x. All images were taken with 1mm scale bar in frame. Images were entered into Adobe Illustrator CC 19.2.1 (Adobe Systems Inc. 2015) and the outer borders of the ray hemitrichs were traced, converted into solid white polygons on a black background and saved as black and white JPEGs for import into Image J version 2.0.0 (Fig. 2B). Scale bars were included as white 1mm lines. ImageJ with Bone J plugin version 1.4.3 was used to determine the centroid of the hemitrichia and second moment of area (*I*; mm^4) around the neutral bending axes. The neutral bending axes were aligned with the rostro-caudal direction and the ventro-dorsal directions used in the three-point bending tests respectively (Doube et al., 2010)(Fig. 2C-F). Second moments of area (*I*) were calculated with the equation below:

$$I = \int x^2 dA \quad (1)$$

where *x* is the orthogonal distance from the centroid to the neutral bending axis and *dA* is the area of the bone segment to one side of the neutral bending axis (Macesic and Summers, 2012; Steven Vogel, 2003; Taft, 2011)(Fig. 2C). It is important to note that a walking-ray consists of two separated hemitrichia and a pectoral fin ray consists of four separated hemitrichia (Fig. 2B). Therefore, a cross section of a walking-ray will have two bone segments, and a cross section of pectoral fin ray will have four (Fig. 2B). Due to this arrangement, some cross sections to one side of the neutral bending axes consisted of multiple pieces of a whole bone segment (Fig. 2D), multiple whole bone segments (Fig. 2E) or a combination of both (Fig. 2F). To address this complexity, we elected to add second moments of area determined for each bony segment to one side of the neutral bending axis, rather than taking the product as if they were one continuous piece. For an instance where two pieces of bone segment in a walking-ray cross section were to one side of the neutral

bending axis (Fig. 2D), we calculated the total second moment of area of the walking-ray using the equation below:

$$I_w = \int (x_1^2 \cdot dA_1) + (x_2^2 \cdot dA_2) \quad (2)$$

where I_W is the second moment of area for the walking-ray, x_1 is the distance orthogonal from the centroid of one segment to the neutral bending axis, dA_1 is the area of that segment of the walking-ray and x_2 and dA_2 simply correspond to the second segment (Fig. 2D). In cases where there were more than two pieces of bone segment to one side of the neutral bending axis (Fig. 2F), we added additional elements *x* and *dA* to *eq. 2* with a sequential subscript. Once *I* was determined, the flexural stiffness (*EI*; Nmm^2) was calculated using data obtained from the three-point bending test with the following equation:

$$EI = \frac{Fl^3}{48y_{max}} \quad (3)$$

where *F* is the force required to displace the ray to the maximum displacement distance, denoted as y_{max} and *l* is the distance between the supporting points of the three point bending rig (Macesic and Summers, 2012; Steven Vogel, 2003)(Fig. 2A). Using the flexural stiffness (*EI; Nmm^2*) and second moment of area (*I; mm^4*) values, we then calculated Young's modulus (*E; GPa*) (Macesic and Summers, 2012).

Statistical Analysis

Mechanical data, including *F* at Y_{max}, *I*, *EI* and *E* were separated by ray type (Walking-ray, WR; pectoral fin ray, PFR) and loading direction (rostro-caudal, RC; ventral-dorsal, VD), and then normalized to fish total length (TL) for interspecific and intraspecific comparisons using SPSS version 24.0 (IBM Corp.) (Table 1). Interspecific comparisons were run using one-way ANOVA with mechanical data as dependent variables and species as fixed factors. In instances where homogeneity of variance was not satisfied, a Welch test for robustness of equality of means was performed (Kohr and Games, 1974)(Table 2). Intraspecific comparisons were performed using one-way ANOVA with mechanical data collected from the fresh specimens as dependent variables and ray type and loading direction as independent variables (1=WRRC, 2=WRVD, 3=PFRRC, 4=PFRVD). In instances when normality and homogeneity of variance were not satisfied, individual non-parametric Kruskal-Wallis tests on ranks were performed (Keselman et al., 1979)(Table 2).

RESULTS

Skeletal Morphology

Based on gross observations, the walking-rays appear to be more robust than the pectoral fin rays (Fig. 2B). The walking-ray and pectoral fin ray hemitrichia are fully segmented into bony blocks in the distal half (Fig. 3). The proximal region exhibits a reduced segmentation to such an extent that the proximal-most end of the hemitrichia takes on a more fused rod-like morphology (Fig. 3). The rod-like proximal halves of the walking-ray hemitrichia become flattened rostrocaudally as they approach the articulation with the pectoral girdle. At that point they turn approximately 25 degrees ventrally from the ray long-axis, enlarge and extend ventrally off the ventral surface of the hemitrichia to form robust triangular processes (ventral hemitrichial processes, VHPs) (Fig. 3A). These processes are referred to as ADS (adductor superficialis) processes in Harris 2013. VHPs are also present on the pectoral fin rays, but they are much smaller. Continuing proximally from the VHPs, the hemitrichia turn approximately 32 degrees dorsally and extend to articulate with the lateral edge of the distal coracoid just distal to the radials (Fig. 4A). At the articulation, the dorsal hemitrich forms a ball-like condyle and the ventral hemitrich forms a curved peg-like process that extends under the ventral edge of the coracoid when the rays are tucked against the body (Fig. 4B). The lateral-facing surface of coracoid that articulates with the rays has shallow cup-like fossa that align with the condyles of the dorsal hemitrichia (Fig. 4B).

The segments of the walking-ray dorsal hemitrich exhibit a unique S-shape that is easily observed when viewed dorsally (Fig. 3C). Each segment has a bony flange that extends distally to overlap the next segment distally in the series, and proximally to overlap the next segment proximally in the series on the rostral and caudal facing edges, respectively (Fig. 3B). The ventral surface of the dorsal hemitrich on the walking-rays is concave (Fig. 3B). This is similar to pectoral fin rays; however, the concavity is not as prominent on the dorsal surface of the ventral hemitrich as it is in the pectoral fin rays. Additionally, there is prominent beveling on the ventral surfaces of both dorsal and ventral walking-ray hemitrichia, which is in contrast to the morphology of the pectoral fin rays (Fig. 3B). It is notable that the CT rendering in Fig. 3A shows a gap between the dorsal and ventral

hemitrichia. This walking-ray was scanned with all connective tissue and skin intact, but it was disarticulated from the pectoral girdle, so it is unclear whether or not this gap is possible *in-vivo*.

Muscular Morphology

The musculature associated with the walking-rays of the two sea-robin species that were used in this study have markedly similar arrangement and architecture. All walking-ray musculature originates from the pectoral girdle and inserts onto the proximal-most portions of the rays that contain the VHPs (Fig. 5). There are no tendons running the length of the walking-rays, all movement is actuated from the base. The musculature associated with the walking-rays is much more distinct and subdivided than that of the pectoral fin rays (Fig. 5). There appear to be little published descriptions of these muscles except one for *Prionotus carolinus* musculature in a thesis, which was used as a guide (Harris, 2013). In this 2013 study by Harris, what we have termed walking-rays are referred to as free rays. Additionally, the muscles are named based on musculature associated with the pectoral fin rays. Here we propose a naming scheme corresponding to these walking-ray muscles function in locomotion. As such, they are placed into functional divisions consisting of protractors, retractors, levators and depressors. A key containing synonymies of these muscles can be found in supplementary table 1. Further naming was based on position and structural attributes. Most muscle divisions contain three muscles (one for each walking-ray) with similar architectures, origins and insertions. Muscle actions were inferred by pulling muscles of fresh specimens down the muscle line of action. By renaming these muscles, we hope to distinguish them from the pectoral fin ray musculature.

Protractors

Walking-ray Protractor Magnus (WPM). The WPM is the largest division of this group and is a singular muscle that is associated with the first walking-ray only (Fig. 5A). It is notable that Harris 2013 described this muscle as part of the division of abductor superficialis (Harris, 2013) (Table S1). We believe it to be its own division, at least in the species studied here, *Prionotus evolans*. This muscle is unipennate and originates on the ventrolateral surface of the distal portion of the coracoid just proximal to the origin of deeper divisions of this muscle group. The fibers course caudolaterally at a slight ventral angle until they converge

upon a tendon that inserts proximally upon the rostrodorsal facing surface of the dorsal hemitrich of the first walking-ray at the location of the VHP (Fig. 5A). *Walking-ray Protractor Deep (WPD).* This deep division of protractors contains three unipennate muscles (one for each walking-ray). These muscles originate upon the ventrolateral surface of the most distal portion of the coracoid, just deep to the origin of the WPM. The fibers course caudolaterally until they converge upon a tendon that inserts onto the rostral facing surface of the VHP on the dorsal hemitrich (Fig. 5A).

Retractors

Walking-ray Retractor Superficial (WRS). The superficial division of the retractors are parallel-fibered and originate on the medial surface of the proximal cleithrum (Fig. 5C). The fibers course rostromedially at a slight ventral angle and insert onto the ventrocaudal surface of the ventral hemitrich, just distal to the VHP. It is notable that the WRS for the third walking-ray is slightly larger than those of the first and second walking-rays (Fig. 5B). *Walking-ray Retractor Deep (WRD).* The deep division of the retractors are bipennate and originate on the medial face of the proximal cleithrum just distal to origins of the superficial divisions. Muscle fibers course rostromedially at a slight ventral angle. Approximately halfway to the insertion, the fibers converge onto the tendon that extends to the ventral hemitrichs of the walking-ray where it inserts onto the caudal facing surface of the end of the triangular VHP. It is notable that the tendon of the WRD crosses over the WRS before inserting onto the VHP (Fig. 5C).

Levators

Walking-ray Levator (WL). The WL muscles are unipennate muscles that originate on the ventral surface of the laterally projecting crest of the mesocoracoid. The fibers course ventrally at a slight rostral angle and converge on a short tendon that inserts onto the dorsal surface of the dorsal hemitrich just distal to the VHPs and the insertion of the WRPs. The WL for the first walking-ray also shares this tendinous connection with the WPM (Fig. 5A).

Depressors

Walking-ray Depressor Superficial (WDS). The superficial division of the depressors consists of three short parallel-fibered muscles which originate from the medial facing surface of

the mesocoracoid. The fibers course caudoventrally to their insertion upon the medial end of the peg-like process at the proximal end of the ventral hemitrich (Fig. 5B). *Walking-ray Depressor Deep (WDD).* The deep division of the depressors consists of three short parallel-fibered muscles that originate from the medial mesocoracoid, just ventral to the origin of the WDS. Fibers extend ventrally to insert onto the dorsal surface of the peg-like processes at the proximal end of the ventral hemitrich (Fig. 5C).

Ray Mobility

At the articulation with the pectoral girdle, both pectoral fin rays and walking-rays have three degrees of freedom: elevation and depression, protraction and retraction, and long axis rotation. Qualitatively, when the pectoral fin rays were manually flexed dorsally, ventrally, rostrally and caudally; they were able to move in all directions with low stiffness. In contrast, when the walking-rays were manually flexed in the same directions as the pectoral fin rays, they resisted flexion in the dorsal, rostral and caudal directions, but not in the ventral direction. This ventral flexing motion of the rays causes one hemitrich to shear past the other.

In order to get a closer look at the behavior of the connective tissue between the dorsal and ventral hemitrichia of the walking-rays, we examined it under a dissecting microscope (Fig. 6). It is notable that a distinct band appeared to connect a bone segment on one hemitrich orthogonally to the associated bone segment on the adjacent hemitrich (Fig. 6A). When the walking-ray was flexed, causing shearing between the two hemitrichia, there was a clear angular shift in the orientation of the connective tissue between the two hemitrichia (Fig. 6B). It was noted that the orthogonal distance between the two hemitrichia decreased during ventral flexion and increased to return to starting length upon relaxation.

The Walking-rays normally rest in a straightened and retracted position against the trunk with distal ends pointing caudally under the pectoral fin. When protracting the rostral-most walking-ray towards the rostrum, the other rays (the second and third walking-rays) followed with the first. When released, all of the rays retracted back into the resting position. Closer inspection of the ventral surface of the rays reveals ligaments that extend from the third to the second walking-ray and from the second to the first walking-ray

(removed in a figure). The ligaments have a broad origin on the rostral surface of the dorsal hemitrich that starts just distal to the articulation with the pectoral girdle and extends parallel to the long axis of the hemitrich, terminating just dorsal to the VHP. The ligament extends from the origin towards the rostral-more ray where it converges and inserts onto the caudal surface of that ray's dorsal hemitrich just dorsal to the VHP. These ligaments become tense when the first walking-ray is protracted, and thus are able to pull the second and third walking-rays into a protracted position. The walking-rays also exhibited automatic ventral flexion when manually protracted or elevated. The rays also auto-extend in the dorsal direction when retracted caudally and depressed.

Mechanical Properties

The force-displacement traces obtained from the three-point bending test shows a steeper slope in both species for the walking-ray in the rostro-caudal direction when compared to the walking-ray in the ventro-dorsal direction (Fig. 7). The slope of the walking-ray in the rostro-caudal direction is also steeper than the slope of the pectoral fin ray in either direction (Fig. 7). A steeper slope in this instance indicates more force applied to displace the ray a distance.

For *Prionotus evolans*, the second moment of area was significantly higher in the walking-ray in both rostro-caudal (0.0835 ± 0.0121 mm^4; Fig. 8A; Table 2) and ventro-dorsal(0.1078 ± 0.0254 mm^4; Fig. 8A; Table 2) directions when compared to the pectoral fin ray in both rostro-caudal (0.0095 ± 0.0034 mm^4, P=0.021;Fig. 8A;Table 2) and ventro-dorsal(0.0153 ± 0.0043 mm^4, P=0.021;Fig. 8A;Table 2) directions. For *Prionotus* carolinus, the walking-ray in the rostro-caudal (0.0447 ± 0.0056 mm^4; Fig. 8A; Table 2) and ventro-dorsal(0.0358 ± 0.0025 mm^4; Fig. 8A; Table 2) directions were also significantly higher than the pectoral fin ray in the rostro-caudal (0.0022 ± 0.0002 mm^4, P=0.003; Fig. 8A;Table 2) and ventro-dorsal(0.0038 ± 0.0003 mm^4, P=0.004; Fig. 8A;Table 2) directions. For the walking-rays of both species and both directions tested, there were no significant differences in the second moments of area (Fig. 8A; Table 2). The flexural stiffness was significantly higher for the walking-rays in the rostro-caudal direction when compared with the walking-ray in the ventro-dorsal direction for both *Prionotus evolans* (P=0.021; Fig. 8B; Table 2) and *Prionotus carolinus* (P=0.004; Fig. 8B; Table 2). It was also significantly higher for the pectoral fin rays in the rostro-caudal and

ventro-dorsal directions for both *Prionotus evolans* (P=0.021; Fig. 8B; Table 2) and *Prionotus carolinus* (P=0.004; Fig. 8B; Table 2). The Young's modulus of the walking-ray in the ventro-dorsal direction was lower for both *P. evolans* and *P. carolinus* (P=0.021 and P=0.004, respectively; Fig. 8C; Table 2).

DISCUSSION

The Unique Morphology of Walking-Rays

Sea-robin walking-rays exhibit a variety of morphological novelties, all of which likely aid in their ability to act as individual limbs and facilitate underwater walking. Several of these features partially support our first hypothesis that the walking-rays will exhibit more robust skeletal components for support and muscle attachment and an increased range of motion at the base compared to pectoral fin rays. The distal portion of the ray is dorsoventrally compressed and the ventral hemitrich has an oval cross-section rather than concave as seen in other fish species (Flammang et al., 2013; Taft, 2011)(Fig. 2B). This shape moves much of the bone material further from rostro-caudal neutral bending axis, which acts to increase the rostro-caudal second moment of area, in turn resulting in reduced rostro-caudal flexibility (Fig. 2; Table 2). Both hemitrichs at the proximal end also transition to solid circular cross-sections, lose the beveling at the junctions of the hemitrich segments and have progressive joint fusion between the segments resulting in a more rod-like morphology prior to reaching the VHPs (Fig. 3A). This is similar to the cylindrical morphology of the proximal portions of the pectoral fin rays of long horn sculpin, *Myoxocephalus octodecimspinosus,* which are thought to have reduced fin ray flexibility as they use them to move along the benthos (Taft, 2011). The circular cross-section of this region in sea-robin is just distal to the insertions of the walking-ray muscles. A circular cross-section results in a consistent distribution of bone regardless of the location of the bending axis through the centroid of the cross-section (Beer, 2013). This would be useful in supporting the rays against loading applied from multiple directions, much like the loads the muscles impose at the base of the walking-rays, as well as the flexion due to contact with the substrate. The pectoral fin rays are not used for walking locomotion, but they have a similar morphology at the proximal end of the rays. This morphology may support the pectoral fin rays in a similar

way; however, instead of the substrate loading the distal end of the ray, loading is increased due to the long length of the rays and hydrodynamic drag on the large wing-like pectoral fin of the sea-robin species studied.

Benefits of S-Shaped Hemitrich Segments

Among the walking-ray morphological novelties described is the s-shape segmentation of the dorsal hemitrich (Fig. 3B). The dorsal hemitrich morphology of the pectoral fin ray in sea-robin are similar to that of typical fin rays, such as the structure found in the bluegill sunfish, *Lepomis macrochirus* (Flammang et al., 2013), in that they are rectangular beveled segments with a concave ventral surface. The walking-ray dorsal hemitrich is minimally concave on the ventral surface and has no rostro-caudal beveling. As a result of the s-shape segmentation found in sea-robins, there are overlapping flanges on the rostral and caudal sides of the joints between the dorsal hemitrich segments (Fig. 3B). The beveling on the rostral and caudal aspects of the dorsal hemitrich has been replaced with these flanges. These flanges help to limit rostro-caudal movement by abutting the next segment in series, rather than folding together like the bevels in pectoral fin rays. We suggest that these features aid in the reduced rostro-caudal flexibility that facilitates underwater walking through transmission of force to the substrate to accelerate the body of the fish (Renous et al., 2000).

There is connective tissue separating the in-series segments of the rays while simultaneously holding them together. Force tending to flex a ray in the rostro-caudal direction would put tensile stress on a section of this connective tissue and stretch it. This assumption uses the same logic as beam bending (Beer, 2013). We suggest that the s-shape segmentation not only provides flanges limiting rostro-caudal flexibility, but also increases the surface area of contact between adjacent segments in-series along the dorsal hemitrich, allowing more area for attachment between the segments (Fig. 3C). This increased attachment area would result in added resistance against tensile forces acting to pull the segments apart. For pectoral fin rays, beveling, the straight rectangular to rectangular abutment, and the overall smaller size all result in a low surface area of contact. In contrast we suggest the lack of beveling, longer s-shape abutment, and larger overall size in the walking-ray provides more surface area for the connective tissue to join segments. This

would, in turn, resist higher tensile forces in the rostro-caudal direction, which work to separate the segments of the walking-ray. Here, we assume that the connective tissue between segments is of the same material in both the pectoral fin ray and walking-ray. We did not identify the type of connective tissue between walking-ray segments in this study, so it is unclear if walking-ray inter-hemitrichial connective tissue is similar or stronger than the connective tissue between pectoral fin ray segments. Further study of this issue is needed.

Muscular Anatomy and Actuation of the Walking-Rays

Manual manipulation and CT analysis supported our hypothesis that the walking-rays would have an increased range of motion at articulation with the pectoral girdle. A notable difference between the pectoral fin ray and walking-ray is the lack of webbing between lepidotrichia in the walking-ray that typically composes the fin membrane (Fig. 1). We suggest that this allows the walking-rays to function as individual appendages rather than one interconnected unit, resulting in greater degrees of freedom at the articulation; three of which were observed total. An advantage of interconnected webbed fin rays is easier locomotion through a fluid environment. This is due to the accompanied large increase in surface area which acts as control surface to facilitate hydrodynamic movement (Shadwick and Lauder, 2006). The loss of this structure may indicate a precursor in the evolutionary transition from water to land, or from fin rays to digits.

While there is no webbing between walking-rays, there are notable ligamentous connections which couple the movements of the three walking-rays together. The effect of these ligaments was observed when protracting the first walking-ray and observing the consecutive protraction of both second and third walking-rays. This linked motion only occurred for protraction. Another place where connective tissue was observed is in between the dorsal and ventral hemitrichia of the walking-ray (Fig. 6). There were significant and distinct orthogonal bands connecting adjacent bone segments. When the walking-ray was flexed ventrally, the bands rotated at an angle and appeared to pull the two hemitrichia closer together as the connective tissue was loaded in tension (Fig. 6B). We suggest that these bands of connective tissue function to provide stability during walking, comparable to how thinner sheets of similarly oriented connective tissue aid in the stiffness of typical fin rays (Alben et al., 2007). Our hypothesis that the walking-ray muscles would be subdivided

and specialized when compared to the pectoral fin ray musculature was supported (Fig. 5). As suggested in Harris 2013, the individual bundles of muscle associated with each walking-ray likely aids in the large range of motion they exhibit. This is compared to the pectoral fin ray musculature, which are not divided into individual muscles bundles for each ray, rather, they are joined loosely by connective tissue (Harris, 2013). In fact, we determined that there are more divisions, including protractors, retractors, levators and depressors, and all of the muscles are notably large in comparison with the musculature associated with pectoral fin rays. These large walking-ray muscles did have additional bony support from various processes on the proximal end of the walking-ray, and notable the VHP (Fig. 3A).

Interestingly, our hypothesis that the walking-rays would have long tendons running down their lengths, similar to the tendons and annular pulleys found in tetrapod digits, was not supported. There were no tendons or ligaments found running the lengths of the walking-rays. This means there must be an alternate mechanism by which the walking-rays are able to undergo flexion. In fact, they are able to undergo flexion in the same way that pectoral fin rays are, even though the degree to which flexion occurs in the walking-rays is much larger. This is achieved by the two hemitrichia sliding past one another while their distal ends are fixed and their proximal ends shift when pulled on by the associated musculature (Alben et al., 2007). We also suggest that rather than being actuated by muscles alone, the flexion can occur due to the arrangement of the articulation with the pectoral girdle, which we observed via manual manipulations in a freshly thawed specimen. The dorsal hemitrich articulates with the pectoral girdle via a ball in socket joint, while the ventral hemitrich articulates with it via a saddle joint. When the walking-ray protracts, the articulation holds the dorsal ball joint in place, while the ventral saddle joints shift, sliding the ventral hemitrich medially past the dorsal hemitrich, thus, causing dorsal-ventral flexion (Fig. 4B). To the best of our knowledge, there are no other naturally occurring biological limbs that can bend and perform complex movements with muscle, tendon and ligament actuation occurring only at the most proximal end.

Mechanical Properties

The final aim of the present study was to quantify the walking-ray flexibility on relevant planes. The rostro-caudal plane was chosen in order to assess stiffness in the direction in which the walking-ray would be loaded during forward locomotion (Renous et al., 2000). The ventro-dorsal plane was chosen as a comparison as it is the primary direction in which the walking-ray is flexible, and this flexion occurs during locomotion (Renous et al., 2000). Our hypothesis that the stiffness of the walking-ray would be the same as the pectoral fin ray, which would necessitate the use of active muscle-modulated stiffness, was at least partially unsupported. The passive stiffness of the walking-ray was significantly higher than that of the pectoral fin ray (Fig. 8; Tables 1, 2). This does not rule out the role that musculature might play in stiffening the walking-rays, but it does suggest the walking-rays are at least passively stiffened by the morphological novelties we highlight. Materials testing via the three-point bending test showed that the walking-rays were stiff in the rostro-caudal direction, and flexible in the ventro-dorsal direction (Fig. 7). These data were then used to calculate specific material properties about each ray. Second moments of area for the walking-rays of two species of sea-robin were significantly higher in each case to their pectoral fin ray counterparts in each direction tested (Fig. 8A; Tables 1, 2).

Since hemitrichia are jointed down their length and the segmentation of the ray varies slightly from proximal to distal, we acknowledge that these composite structures do not represent true beams. Although Euler-Bernoulli Beam theory assumes a homogeneous and continuous beam, applying physics to biological systems and deriving these measurements from fin rays is not a new practice (Kato and Kamimura, 2008; Shadwick and Lauder, 2006; Taft, 2011; Weickhardt et al., 2017). We acknowledge the limitations but suggest that the data from these calculations provide a representative quantification of observed qualitative function, despite some intrinsic error that we highlight is present.

We also recognize that the high second moment of area for the walking-ray could be largely due to the increased size when compared to the pectoral fin ray (Fig. 2B). We do not believe this discounts our measure of a high second moment of area for the walking-ray; the third walking-ray is located adjacent to the first pectoral fin ray, the size

difference between the two was consistent between all individuals measured suggesting that the walking-rays might have evolved to be larger and more robust. One result of a large walking-ray cross section here is an increased second moment of area, which is a functionally significant adaptation in this instance. Measures of flexural stiffness also show that the walking-rays are stiffer in the rostro-caudal direction than the ventro-dorsal direction, and stiffer than the pectoral fin rays in either direction (Fig. 8B; Tables 1, 2). The walking-ray and pectoral fin ray are a composite, presumably made from the same material. Thus, even though the shape and stiffness of the walking-ray and pectoral fin ray are different, if they are in fact made from the same material, their Young's modulus should not be significantly different. This is what we observed, the Young's modulus for the walking-ray in the rostro-caudal was not significantly higher than the pectoral fin ray modulus in the rostro-caudal direction (Fig. 8C; Tables 1, 2). The lack of significant differences in our result therefore suggests that it is the structure that is affecting the stiffness and not the material. This highlights the structural novelties we present as a primary source for rostro-caudal stiffness in the walking-ray. Notably, the Youngs modulus for the walking-ray in the ventro-dorsal was significantly low in both species when compared to the pectoral fin ray (Fig. 8C; Tables 1, 2). This result might suggest that the walking-ray is composed of a different material than the pectoral fin ray, especially in areas relevant to the ventro-dorsal neutral bending axis, such as the inter-hemitrichial connective tissue or connective tissue between in-series bone segments. However, given the violations of the Euler-Bernoulli Beam theory assumptions, and the large increase in beveling on the ventral aspect of the ventral walking-ray hemitrich, it is possible that the low modulus is a result of this structure not representing a true beam. This area was beyond the scope of the current study and should be explored in future work.

Uncoupling of Locomotion and Feeding

It is interesting to consider the many possible benefits of these types of walking appendages that are found in sea-robins. Future studies looking at the muscle activation or the energetics of underwater walking compared to swimming might provide valuable insight into some potential advantages to this strategy. One possibility is locomotion using these walking appendages may be less metabolically costly than lateral undulation through the water column. They could also provide additional benefits when foraging for food. Sea-

robins are known to feed on benthic prey, and typically use the walking-rays to probe the seafloor as they walk (Morrill, 1895). Swimming close to the seafloor while undulating their body may stir up sediment, making navigation and prey detection challenging. The walking-rays may improve prey detection two-fold by reducing sediment disturbance caused from swimming as well as using their known sensory receptors located along the walking-rays to more easily locate nearby prey (Eudes-Deslongchamps, 1843; Morrill, 1895).

It is also possible the use of walking-rays during foraging may allow for powerful suction feeding to occur simultaneously with locomotion. It is well known that the epaxial and hypaxial muscles of fish contribute to lateral undulation for swimming (Jayne and Lauder, 1995; Jimenez and Brainerd, 2020; Webb, 1982). However, recent studies suggest these muscles also generate a majority of the power for suction feeding (Camp et al., 2015; Jimenez and Brainerd, 2020). Jimenez & Brainerd found that largemouth bass modulate the dual function of their trunk muscles by selectively activating different regions for each behavior. They speculate that there are inherent tradeoffs between swimming and powerful suction feeding as both behaviors can require recruiting all regions of the trunk musculature (Jimenez and Brainerd, 2020). Based on this, trunk muscles likely switch tasks, and this task switching may incur some delay, requiring a brief pause in locomotion to powerfully suction feed. This highlights the potential inability for the trunk musculature to undulate simultaneously while powerfully suction feeding. We suggest that the presence of walking-rays in the sea-robin may allow them to avoid this temporary pause in locomotion when suction feeding as it moves the muscular source of locomotion to the walking-ray musculature. This would allow the trunk muscles to be entirely devoted to feeding during walking.

Conclusion

Underwater walking evolved in many fish lineages (Dickson and Pierce, 2019; Edwards, 1989; King et al., 2011), but the method employed by sea-robins is unique among them in that it is the only method to use free fin rays as the sole structures for walking. Surprisingly, these walking-rays are arranged similar to typical fins rays in that they are bony lepidotrichia composed of two segmented (chain-like) hemitrichia. Close examination of the walking-ray hemitrichia reveals many structural novelties such as S-shaped hemitrichial segments,

increased ventral beveling to the segments, and changes in cross-sectional geometry. These small-scale changes to the ray morphology have resulted in a chain-like structure with increased stiffness on the rostro-caudal plane. This promotes force transfer to the substrate while maintaining flexibility ventrally so the rays can be flexed to contact the substrate and prop-up the body. The walking-rays are also able to rotate about their long axis, which seems to be due to their separation from the pectoral fin membrane as well as the presence of a ball-and-socket articulation with the pectoral girdle. The walking-ray musculature is separated from the pectoral fin musculature and inserts onto large ventral hemitrichial processes (VHPs) that should increase the moment arms of the muscular. However, the musculature does not seem as if it would directly affect ray stiffness as they all insert at the proximal ends of the rays, very close to the articulation. Together these morphological adaptations result in a lightweight collapsible appendage that is rigid in the direction that promotes their use as a structure for walking.

LIST OF ABBREVIATIONS

WR(s)	Walking-ray(s)
PFR(s)	Pectoral fin ray(s)
RC	Rostro-caudal
VD	Ventro-dorsal
VHP	Ventral hemitrichial process
WPM	Walking-ray protractor magnus
WPD	Walking-ray protractor deep
WRS	Walking-ray retractor superficial
WRD	Walking-ray retractor deep
WL	Walking-ray levator
WDS	Walking-ray depressor superficial
WDD	Walking-ray depressor deep

ACKNOWLEDGMENTS

We gratefully thank Adam Summers for the use of the University of Washington Friday Harbor Laboratories' MTS system and CT scanner, Elizabeth Brainerd for preforming the CT scans, Jennifer Hanselman, Lamis Jarvinen and Westfield State University for support and outreach associated with the research, Kory Evan for assistance analyzing the CT scans and two anonymous reviewers whose comments significantly improved the quality of the manuscript. We also thank Glen Brewster, Kelly Ann McKeown, Thomas Roberts, Ethan Wold, Mary Kate O'Donnell, Yordano Jimenez, Marisa Agarwal and the 2018 Summer Friday Harbor Fish Class for helpful discussion and comments that greatly improved the manuscript.

COMPETING INTERESTS

The Authors declare no competing or financial interests.

FUNDING

This research was supported by the Center for Undergraduate Research and Creative Activity (CURCA), Honors Program, Institutional Advancement, and Student Affairs Departments of Westfield State University.

DATA AVAILABILITY

The data that support the findings of this study are available from the corresponding author upon reasonable request.

LITERATURE CITED

Alben, S., Madden, P. G. and Lauder, G. V. (2007). The mechanics of active fin-shape control in ray-finned fishes. *J. R. Soc. Interface* **4**, 243–256.

Beer, F. P. (2013). *Vector Mechanics for Engineers (10th ed.)*. New York: McGraw-Hill.

Bilecenoglu, M. and Ekstrom, L. J. (2013). Pelvic fin walking and punting behaviour of raja radula delaroche, 1809 observed in the sea of marmara. *Mediterr. Mar. Sci.* **14**, 158–161.

Camp, A. L., Roberts, T. J. and Brainerd, E. L. (2015). Swimming muscles power suction feeding in largemouth bass. *Proc. Natl. Acad. Sci. U. S. A.* **112**, 8690–8695.

Dickson, B. V. and Pierce, S. E. (2019). How (and why) fins turn into limbs: Insights from anglerfish. *Earth Environ. Sci. Trans. R. Soc. Edinburgh* **109**, 87–103.

Doube, M., Klosowski, M. M., Arganda-Carreras, I., Cordelières, F. P., Dougherty, R. P., Jackson, J. S., Schmid, B., Hutchinson, J. R. and Shefelbine, S. J. (2010). BoneJ: Free and extensible bone image analysis in ImageJ. *Bone* **47**, 1076–1079.

Doyle, J. R. (1988). Anatomy of the finger flexor tendon sheath and pulley system. *J. Hand Surg. Am.* **13**, 473–484.

Edwards, J. L. (1989). Two perspectives on the evolution of the tetrapod limb. *Integr. Comp. Biol.* **29**, 235–254.

Eudes-Deslongchamps, E. (1843). Observations pour servir a l'observation anatomique et physiologique des Trigles. *Mem Soc Linn Normandie* 45–52.

Flammang, B. E., Alben, S., Madden, P. G. A. and Lauder, G. V. (2013). Functional morphology of the fin rays of teleost fishes. *J. Morphol.* **274**, 1044–1059.

Harris, J. P. (2013). The Comparative Morphology of the Pectoral Free Rays in Scorpaenoid Fishes (perciformes: Scorpaenoidea). *Master's Theses* **1457**,.

Hennebert, E., Haesaerts, D., Dubois, P. and Flammang, P. (2010). Evaluation of the different forces brought into play during tube foot activities in sea stars. *J. Exp. Biol.* **213**, 1162–1174.

Hu, D. L. and Bush, J. W. M. (2010). The hydrodynamics of water-walking arthropods. *J. Fluid Mech.* **644**, 5–33.

Jayne, B. C. and Lauder, G. V. (1995). Are muscle fibers within fish myotomes activated synchronously? Patterns of recruitment within deep myomeric musculature during

swimming in largemouth bass. *J. Exp. Biol.* **198**, 805–815.

Jimenez, Y. E. and Brainerd, E. L. (2020). Dual function of epaxial musculature for swimming and suction feeding in largemouth bass. *Proc. R. Soc. B Biol. Sci.* **287**,.

Kato, N. and Kamimura, S. (2008). *Bio-mechanisms of Swimming and Flying: Fluid Dynamics, Biomimetic Robots, and Sport Science*. Japan: Springer.

Keselman, H. J., Games, P. A. and Rogan, J. C. (1979). Protecting the overall rate of Type I errors for pairwise comparisons with an omnibus test statistic. *Psychol. Bull.* **86**, 884–888.

King, H. M., Shubin, N. H., Coates, M. I. and Hale, M. E. (2011). Behavioral evidence for the evolution of walking and bounding before terrestriality in sarcopterygian fishes. *Proc. Natl. Acad. Sci. U. S. A.* **108**, 21146–21151.

Kohr, R. L. and Games, P. A. (1974). Robustness of the analysis of variance, the welch procedure and a box procedure to heterogeneous variances. *J. Exp. Educ.* **43**, 61–69.

Lauder, G. V., Madden, P. G. A., Mittal, R., Dong, H. and Bozkurttas, M. (2006). Locomotion with flexible propulsors: I. Experimental analysis of pectoral fin swimming in sunfish. *Bioinspiration and Biomimetics* **1**,.

Macesic, L. J. and Summers, A. P. (2012). Flexural stiffness and composition of the batoid propterygium as predictors of punting ability. *J. Exp. Biol.* **215**, 2003–2012.

Morrill, A. D. (1895). The Pectoral Appendages of Prionotus and their Innervation. *J. Morphol.* 177–191.

Nakamura, T., Gehrke, A. R., Lemberg, J., Szymaszek, J. and Shubin, N. H. (2016). Digits and fin rays share common developmental histories. *Nature* **537**, 225–228.

Renous, S., Gasc, J. P., Bels, V. L. and Davenport, J. (2000). Six-legged walking by a bottom-dwelling fish. *J. Mar. Biol. Assoc. United Kingdom* **80**, 757–758.

Shadwick, R. E. and Lauder, G. V. (2006). *Fish Biomechanics*. San Diego: Elsevier.

Steven Vogel (2003). *Comparative Biomechanics: Life's Physical World*. Princeton, NJ: Princeton University Press.

Taft, N. K. (2011). Functional implications of variation in pectoral fin ray morphology between fishes with different patterns of pectoral fin use. *J. Morphol.* **272**, 1144–1152.

Walker, J. A. (2004). Kinematics and performance of maneuvering control surfaces in teleost fishes. *IEEE J. Ocean. Eng.* **29**, 572–584.

Webb, P. W. (1982). Locomotor Patterns in the Evolution of Actinopterygian Fishes. *Society* **342**, 329–342.

Weickhardt, A. F., Feilich, K. L. and Lauder, G. V. (2017). Structure of supporting elements in the dorsal fin of percid fishes. *J. Morphol.* **278**, 1716–1725.

Yano, T. and Tamura, K. (2013). The making of differences between fins and limbs. *J. Anat.* **222**, 100–113.

Figures

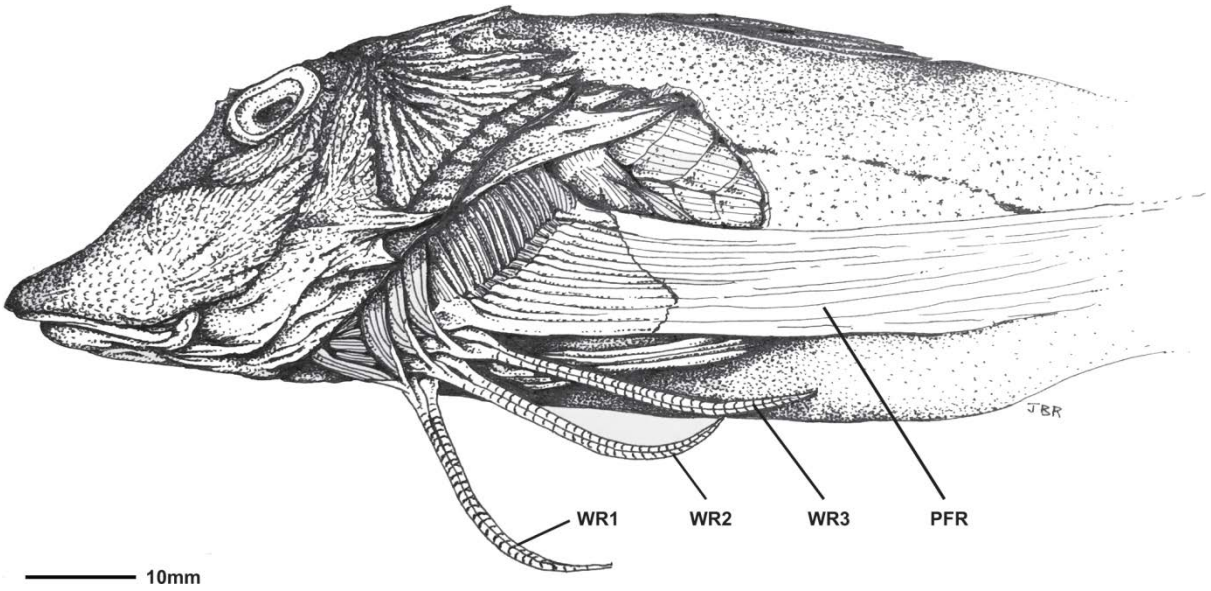

Figure 1: Illustration of the striped sea-robin, *Prionotus evolans*. A lateral view of the left side is shown from the most caudal portion to just before the anal fin. The skin surrounding the left pectoral girdle, walking-rays, proximal fin rays and a portion of the body is removed to reveal the underlying musculature, ligaments and bone. WR1, WR2 and WR3 correspond to walking-rays 1, 2 and 3 respectively. A pectoral fin ray is labeled as PFR.

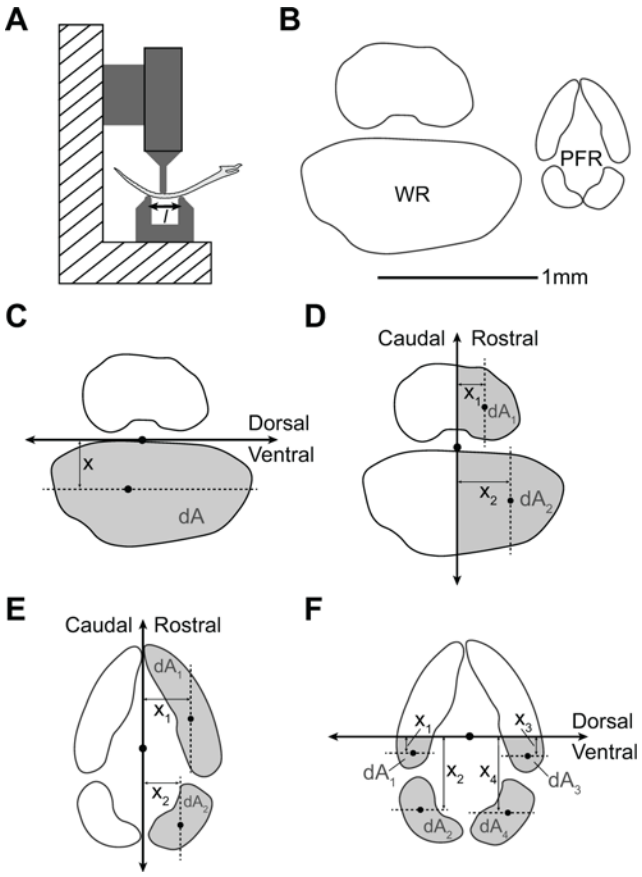

Figure 2: Mechanical and Material Properties. A three-point bending rig is shown (A) with three round points of contact. The upper dark gray section of the schematic is movable to produce variable displacement in the ray. This section housed the MTS 50-gram load cell. Distance *l* is shown with the black arrow as the distance between the bottom two points of stationary contact. A walking-ray is illustrated in the ventral-dorsal direction between the three points of contact. A cross section of the walking-ray and pectoral fin ray shown to scale (B), taken at the middle point of force application from the three-point bending rig. Cross sections of walking-rays (C, D) and pectoral fin rays (E, F) are shown with various neutral bending axes along the ventral-dorsal (C, F) and rostro-caudal (D, E) planes. The neutral bending axes are shown via thick black arrows with the corresponding directions located to either side of the arrow. The shaded regions (C-F) represent the area of each segment *dA* to one side of the neutral bending axis. The approximate centroid of each cross section and segment to one side of the neutral axis is marked with a black circle and *x* corresponds to the distance orthogonal from the centroid to the neutral bending axis. Among these variables, subscripts indicate the number of segments located to one side of

the neutral bending axis, and to which segment the variable belongs. For example, the fourth segment in (F) which is floating in the bottom right of the illustration has the corresponding x value of x_4 and dA value of dA_4.

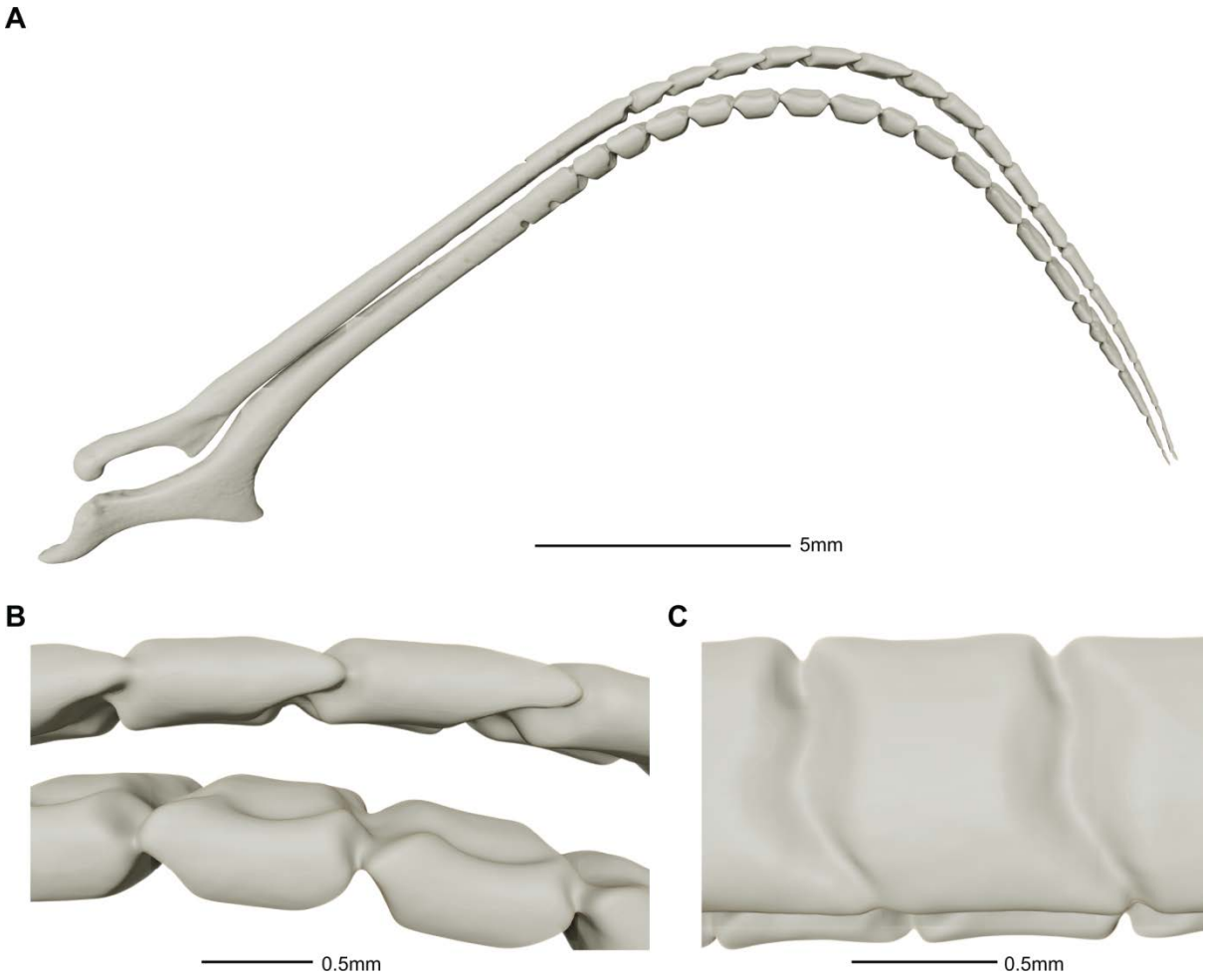

Figure 3: Bone morphology of an individual flexed walking-ray. The left first walking-ray is shown flexed ventrally from a rostral view (A). The ventral hemitrichial process (VHP) is visible at the proximal end of the ventral hemitrich in this view, as well as the differences in segmentation along the hemitrichia from proximal to distal. The middle of this same ray is shown magnified from the same rostral view depicting the overlapping processes of each bone segment and the morphology of each hemitrich (B). This magnified view of the middle of the walking-ray is then observed from a superior view highlighting the S-shape bone segmentation of the dorsal hemitrich (C). It is notable that although the hemitrichia appear as one piece, there is separation between each segment that is hidden due to a lack of resolution. Each ray that scanned had all skin and connective tissue intact.

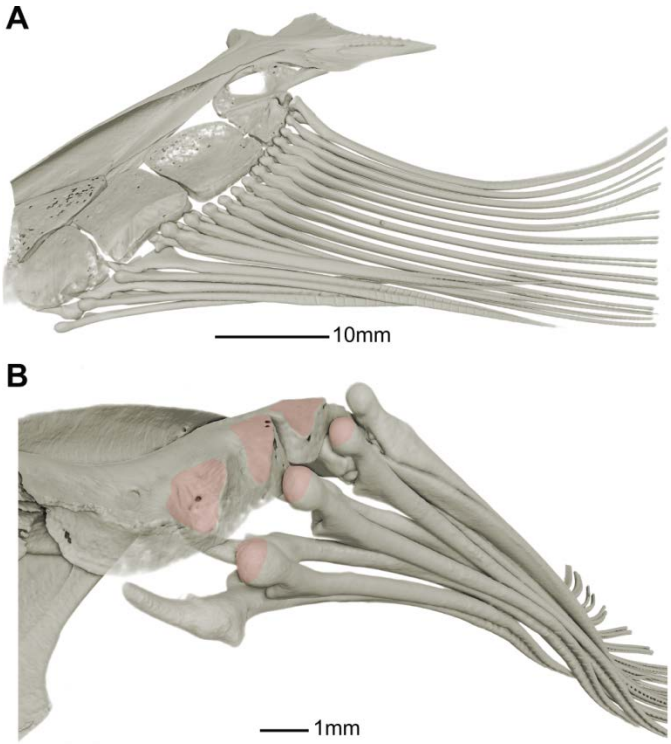

Figure 4: Pectoral girdle morphology of the sea-robin. The right pectoral girdle is shown with pectoral fin rays and walking-rays 1-3 attached. The ends of the pectoral fin rays were not in the window of the scanner and appear cut off in each image. The pectoral girdle is shown in a lateral and slightly ventral view (A) as well as a magnified caudal ventral view (B). The heads of the dorsal hemitrichia and their articulations with the pectoral girdle are highlighted in red (B). It is important to note that the 1mm scale bar, due to the three dimensional nature of the image, applies to only the plane where the heads of the walking rays and their articulations are highlighted in red. The large amount of space between the articulations in this view is likely due to soft tissue which is hidden from view.

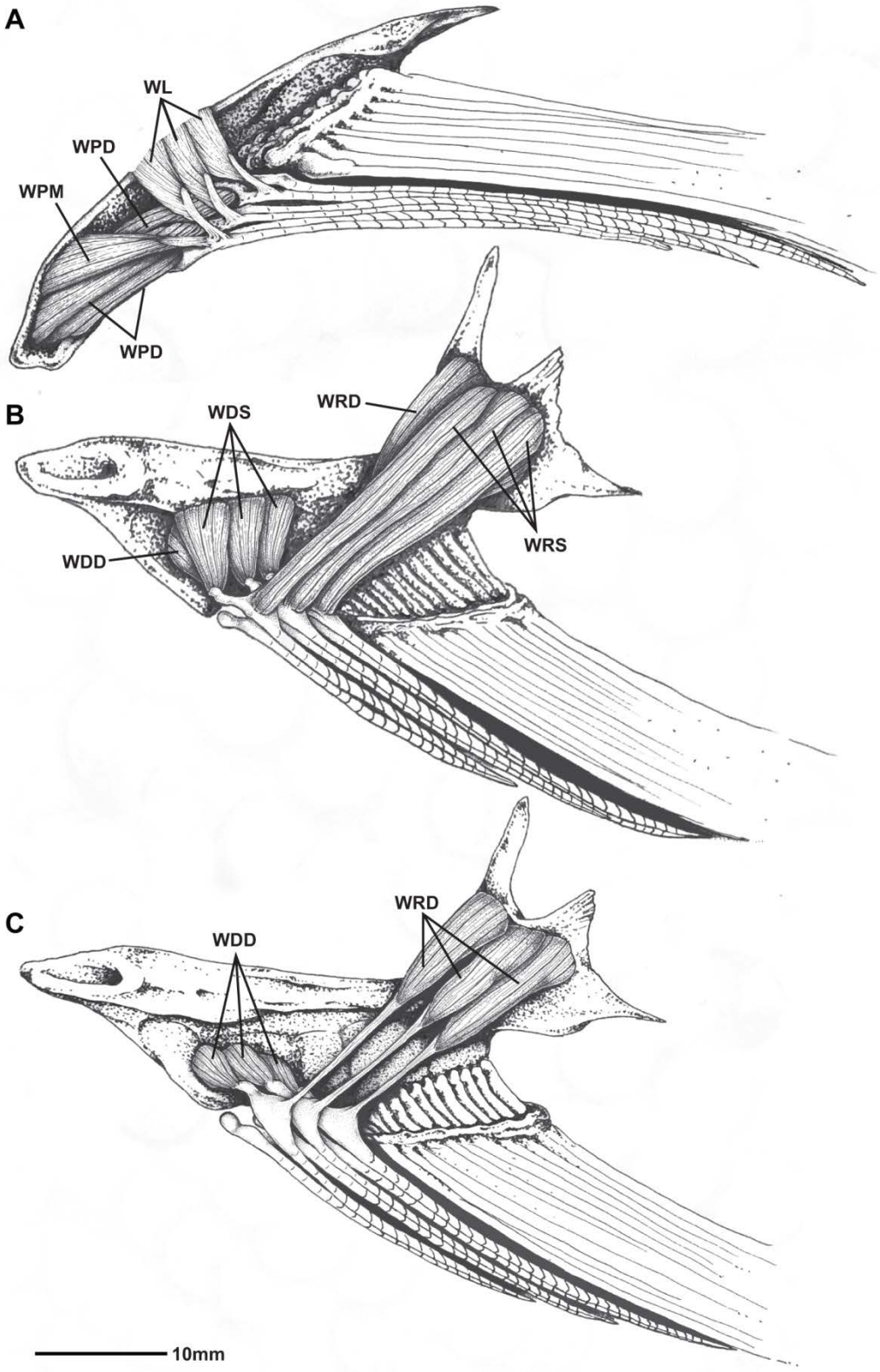

Figure 5: Musculature of the walking-rays associated with the pectoral girdle. A lateral view of an illustration of the isolated left pectoral girdle is shown (A). The walking-ray

protractor magnus (WPM) is shown covering most of the deep walking-ray protractors (WPD). Just superior, the walking-ray levators are visible (WL). The deep side of the pectoral girdle is shown (B) with the superficial walking-ray depressors (WDS) and superficial walking-ray retractors in view (WRS). The deep walking-ray depressors (WDD) and deep walking-ray retractors (WRD) can be seen here but are more easily viewed when the WDS and WRS are removed (C).

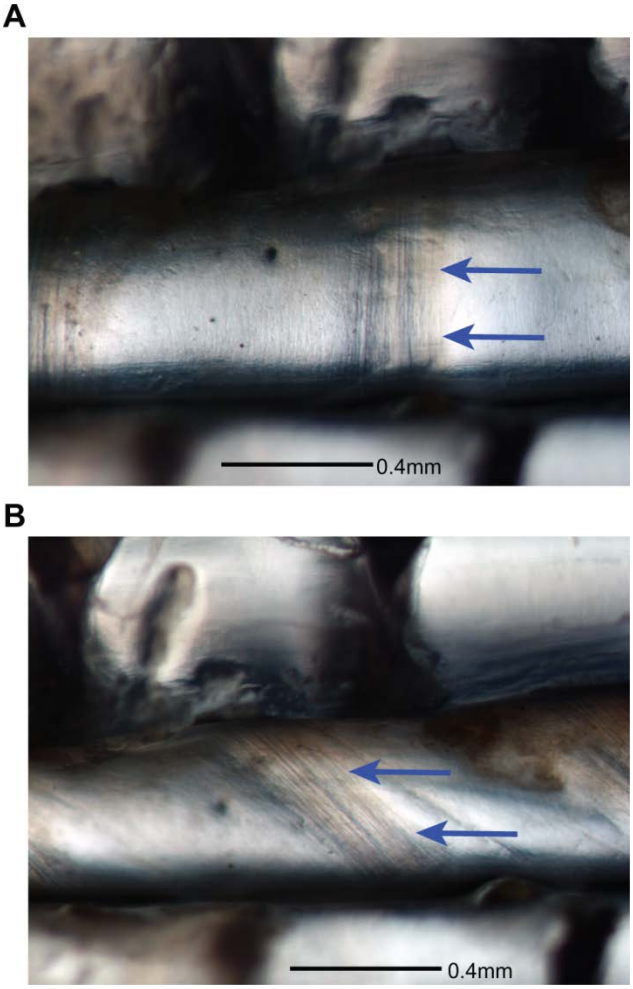

Figure 6: Inter-hemitrichial connective tissue. Two images from a dissecting scope are shown of the space between the medial region of the ventral and dorsal hemitrichia. The ray was photographed in a relaxed (A) and ventrally flexed (B) position. The distinct band of connective tissue attaching corresponding bone segments between the ventral and dorsal hemitrichia are marked by dark blue arrows. These bands can be seen rotating to an angle when the two hemitrichia shear past one another. The superior part of each image represents the ventral hemitrich which slides over the dorsal hemitrich when ventrally flexed.

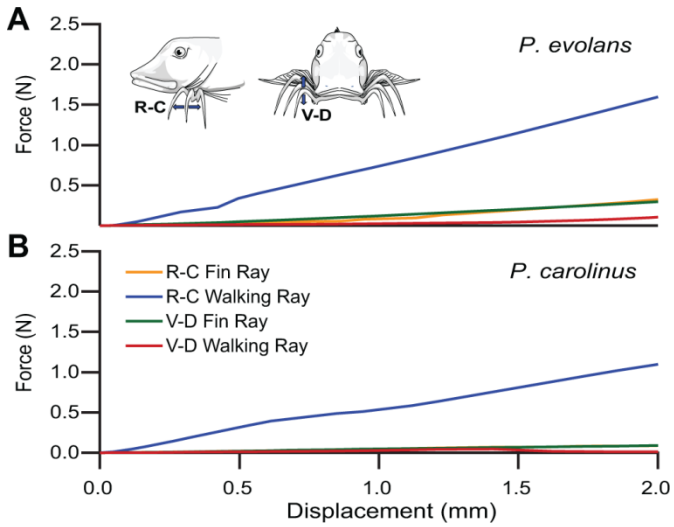

Figure 7: Force-displacement curves obtained from the three-point bending test.

Representative data from *P. evolans* (n=1) (A) and *P. carolinus* (n=1) (B) are shown. In all cases, force increases with displacement as expected. The lines are color-coded for direction and type of ray. rostro-caudal corresponds to rostro-caudal and ventro-dorsal corresponds to ventral-dorsal, as indicated in the inset drawing.

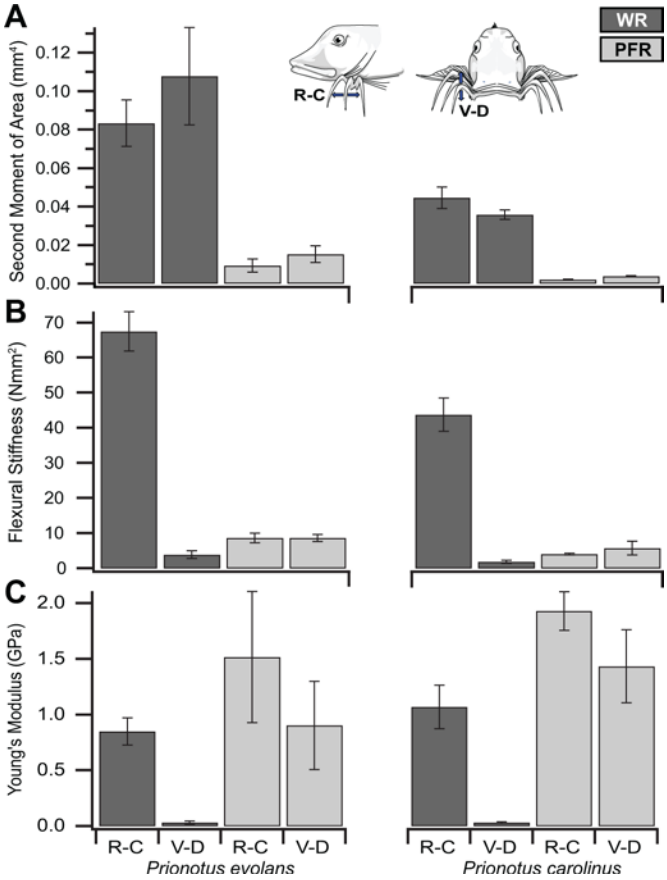

Figure 8: Mechanical properties of the walking-rays and fin rays. The second moment of area (*I; mm*^{4}) (A), flexural stiffness (*EI; Nmm*^{2}) (B) and Young's modulus (*E; GPa*) (C) are reported in the left column for *P. evolans* (n=4) and in the right column for *P. carolinus* (n=6) (means ±s.d.). The dark grey bars correspond to the walking-rays, and the light gray bars correspond to the pectoral fin rays. The rostro-caudal direction is represented by the inset and data labeled RC, the ventral-dorsal direction is represented by the inset and data labeled VD. The exact values for these data are reported in Table 1, and the statistics for these data are reported in Table 2.

TABLES

TABLE 1. Mechanical Properties of Sea-robin Walking and Pectoral Fin rays

Sea-robin Species	Ray Type	Loading Direction	Load *F (N)*	SMoA *I (mm^4)*	Flexural Stiffness *EI (Nmm^2)*	Young's Modulus *E (Gpa)*
Prionotus evolans	WR	RC	1.1180 ± 0.1088	0.0835 ± 0.0121	67.4978 ± 5.6011	0.8500 ± 0.1223
		VD	0.0647 ± 0.0189	0.1078 ± 0.0254	3.9278 ± 1.1317	0.0306 ± 0.0145
	PFR	RC	0.1407 ± 0.0212	0.0095 ± 0.0034	8.6668 ± 1.3256	1.5167 ± 0.5890
		VD	0.1410 ± 0.0158	0.0153 ± 0.0043	8.6865 ± 1.0288	0.9032 ± 0.3969
Prionotus carolinus	WR	RC	0.7090 ± 0.0756	0.0447 ± 0.0056	43.7680 ± 4.7639	1.0701 ± 0.1945
		VD	0.0320 ± 0.0070	0.0358 ± 0.0025	1.8997 ± 0.4131	0.0317 ± 0.0069
	PFR	RC	0.0666 ± 0.0038	0.0022 ± 0.0002	4.0640 ± 0.2442	1.9298 ± 0.1733
		VD	0.0937 ± 0.0304	0.0038 ± 0.0003	5.7513 ± 1.9299	1.4332 ± 0.3277

Means±s.e.m.; PFR, pectoral fin ray; RC, rostro-caudal; VD, ventral-dorsal; WR, walking-ray.

P. evolans (n=4) and *P. carolinus* (n=6).

TABLE 2. Results of Individual Kruskal-Wallis Tests on Ray Type and Loading Direction (a=0.05)

Sea-robin Species	Ray Type	Loading Direction	RD#	Comparison	Load *F (N)*		SMoA *I (mm^4)*		Flexural Stiffness *EI (Nmm^2)*		Young's Modulus *E (Gpa)*	
Prionotus	WR	RC	1	1-2	**P=0.021**	**1>2**	P=0.564	1=2	**P=0.021**	**1>2**	**P=0.021**	**1>2**
evolans		VD	2	1-3	**P=0.021**	**1>3**	**P=0.021**	**1>3**	**P=0.021**	**1>3**	P=0.386	1=3
	PFR	RC	3	1-4	**P=0.021**	**1>4**	**P=0.021**	**1>4**	**P=0.021**	**1>4**	P=0.248	1=4
		VD	4	2-3	P=0.083	2=3	**P=0.021**	**2>3**	P=0.083	2=3	**P=0.021**	**2<3**
				2-4	P=0.083	2=4	**P=0.021**	**2>4**	P=0.083	2=4	**P=0.021**	**2<4**
				3-4	P=0.564	3=4	P=0.248	3=4	P=0.564	3=4	P=0.248	3=4
Prionotus	WR	RC	1	1-2	**P=0.004**	**1>2**	P=0.146	1=2	**P=0.004**	**1>2**	**P=0.004**	**1>2**
carolinus		VD	2	1-3	**P=0.004**	**1>3**	**P=0.003**	**1>3**	**P=0.004**	**1>3**	**P=0.010**	**1<3**
	PFR	RC	3	1-4	**P=0.004**	**1>4**	**P=0.004**	**1>4**	**P=0.004**	**1>4**	P=0.423	1=4
		VD	4	2-3	**P=0.004**	**2>3**	**P=0.003**	**2>3**	**P=0.004**	**2>3**	**P=0.004**	**2<3**
				2-4	**P=0.016**	**2>4**	**P=0.004**	**2>4**	**P=0.016**	**2>4**	**P=0.004**	**2<4**
				3-4	P=1.000	3=4	**P=0.004**	**3>4**	P=1.000	3=4	P=0.078	3=4

PFR, pectoral fin ray; RC, rostro-caudal; VD, ventral-dorsal; WR, walking-ray. *P. evolans* (n=4) and *P. carolinus* (n=6).

Table S1. *Synonymies of muscles described for* Prionotus *evolans and* Prionotus carolinus *(Harris 2013)*

Click here to Download Table S1